Author's Accepted Manuscript

www.elsevier.com/locate/talanta

Three-dimensional Tri-SNSs-layered electrodeposited reduced graphene oxide for ECL biosensing of DNA

Yaoyu Wu, Jianying Yang, Zengyao Zheng, Zuoqiu Li, Fusheng Lu, Yaowen Chen, Wenhua Gao

PII: S0039-9140(18)30538-1
DOI: https://doi.org/10.1016/j.talanta.2018.05.045
Reference: TAL18686

To appear in: *Talanta*

Received date: 3 February 2018
Revised date: 5 May 2018
Accepted date: 11 May 2018

Cite this article as: Yaoyu Wu, Jianying Yang, Zengyao Zheng, Zuoqiu Li, Fusheng Lu, Yaowen Chen and Wenhua Gao, Three-dimensional Tri-SNSs-layered electrodeposited reduced graphene oxide for ECL biosensing of DNA, *Talanta,* https://doi.org/10.1016/j.talanta.2018.05.045

Three-dimensional Tri-SNSs-layered electrodeposited reduced graphene oxide for ECL biosensing of DNA

Yaoyu Wu[a,b], Jianying Yang[b], Zengyao Zheng[b], Zuoqiu Li[a], Fusheng Lu[a], Yaowen Chen[c], Wenhua Gao[a,c*]

[a]Department of Chemistry and Laboratory for Preparation and Application of Ordered Sructural Materials of Guangdong Province, Shantou University, Shantou, Guangdong 515063, P. R. China

[b]National Detergents and Cosmetics Products Quality Supervision and Inspection Center (Guangdong), Shantou, Guangdong 515041, P. R. China

[c] Analysis & Testing Center, Shantou University, Shantou, Guangdong 515063, P. R. China

[*]Corresponding author. Tel: +86-22-86502774; Fax: +86-22-82903941. whgao@stu.edu.cn

Abstract

In this study，we proposed a triangular silver nanosheets (Tri-SNSs)-layered, Chitosan (CS)-supported three-dimensional of reduced graphene oxide (3D-ERGO) electrochemiluminescence (ECL) biosensing platform using self-designed dual-Ru(bpy)$_3^{2+}$ scDNA (Ru_2-DNA) as capture probe for ECL biosensing of single-chain DNA (scDNA). Based on the different affinity with scDNA and double chain DNA (dcDNA), the biosensor is designed to recognize the target DNA (t-DNA), which leads to the desorption of a hybrid molecule from the surface of the biosensor, further removing the Ru_2-DNA and inhibiting the ECL. Analytical results clearly showed that the electrochemical and ECL behaviors of proposed biosensing platform on the glassy carbon electrode (GCE) exhibited outstanding performance, which was due to large specific surface area, high carrier mobility and strong π–π non-covalent attraction toward single-chain DNA (scDNA) of the stable 3D platform, and ECL amplification of Tri-SNSs. Besides, based on such a system, this strategy can effectively identify full match and mismatched target DNA (M-DNA) with a wide concentration range beyond 7 orders of magnitude and detection limit down to 16.2

aM. Therefore, the 3D biosensing strategy shows potential for the application of bioassays.

Key words: 3D-ERGO; Tri-SNSs; Ru_2-DNA; t-DNA; ECL; biosensor.

1. Introduction

With in-depth research in biochemical technology, hypersensitivity testing of low-concentration specific DNA sequences has recently shown a far-reaching significance and potential application in biological studies. These studies include the diagnosis of genetic disease and precancerous lesion, environmental monitoring, as well as bacterial and parasitic infection. [1,2,3] Moreover, DNA research has contributed to the development of other disciplines and opened significant opportunities for future research. Owing to these significance and intrinsic values, numerous DNA detection techniques based on the hybridization of a probe DNA and its complementary target have drawn interest [4]. Fluorescence [5,6], electrochemistry [7,8], Chemiluminescence[9], ECL [10,11], quartz–crystal microbalance [12], surface plasmon resonance [13], and surface-enhanced raman scattering [14] are of vital significance for a specific DNA sequence. However, owing to its low background signals, significant electrochemical stability, unparalleled biocompatibility, and high luminous efficiency, electrochemiluminescence has stood out from numerous analytical techniques and recently become a high-profile analytical method [15]. First discovered by Lytle et al. [16], tris(2,2′-bipyridine)-ruthenium(II) ($Ru(bpy)_3^{2+}$), red-orange to red, with outstanding ECL characteristic, extremely high water solubility and excellent chemical stability became a good choice for ECL biosensors preparation to apply to the analysis of target in various samples [17]. Besides, it has drawn increased scientific interest attributed to its superior sensitivity, linear range, and stability with the interaction of tri-n-propylamine (TPA) co-reactants. The maturation of the $Ru(bpy)_3^{2+}$/TPA ECL system further facilitates the detection of specific DNA sequence by the complementary pairing principle of DNA using single-stranded DNA (scDNA) with a $Ru(bpy)_3^{2+}$ as the capture probe and TPA as the

co-reactants. Meanwhile, with the participation of TPA co-reactants, a positive correlation between the intensity of the ECL signal and $Ru(bpy)_3^{2+}$ concentration can be observed. In order to improve the amount of luminescent materials on the sensing platform, many efforts have been made from the redox mechanism and the sensing platform structure. This indicates that $Ru(bpy)_3^{2+}$ is modified only at one end of the scDNA, which results in the other end becoming wasted. Besides，One study mentioned that the $Ru(bpy)_3^{2+}$ could be immobilised at the molecular level onto the electrode surface to improve the effect of ECL, because this prevents the difusion of the generated active species into the bulk.[18] Thus, the combination of $Ru(bpy)_3^{2+}$ and DNA is particularly suitable for biosensing. The design of scDNA with $Ru(bpy)_3^{2+}$ at both ends is encouraged to enhance the ECL signal in the application of biochemical analysis.

Graphene has been regarded as one of the “popular stars” and a promising candidate for advanced sensing applications [19] because of its numerous excellent properties [20], such as lowest electrical resistivity, distinct electronic transport properties, excellent mechanical strength, high compatibility to biomolecules and absorption toward scDNA. [21,22,23,24,25,26] Typically, graphene has been considered an excellent platform for scDNA detection based on different affinities with scDNA and dcDNA [27]. However, under strong π–π interactions and Van der Waals forces, graphene is typically stacked and agglomerated [28]. Moreover, most designs of the ECL DNA biosensors are confined to two-dimensional (2D) graphene, which considerably impedes the improvement of biosensors in structural optimization. With an enlarged specific surface area and increased catalytic activity [29, 30, 31], 3D graphene has drawn significant attention in ECL detection because it can markedly improve the sensitivity to and efficiency of detection of the biosensor. In the preparation of a considerable 3D graphene network substrate, various structured methods have been developed. Compared with the gel [32], hydrothermal, [33] and template [34] methods, the amperometric I–T curve technique provides a more promising alternative assay as a rapid and efficient deposition technique exhibiting advantages, such as low cost, pollution, and power. Chitosan (CS) is employed to

reinforce the stability of materials on the electrode surface by its own film-forming properties, presenting a distinct structural maintenance [35], and thus acquiring a much more stable 3D structure. In addition, the application of CS for DNA immobilization requires neither mercapto–DNA [36] nor biotin–DNA [37], which can result in strong absorption with the polyanionic phosphodiester backbones of scDNA [38] and effectively reduce the cost of t-DNA detection.

Noble metal nanomaterials are widely used as a class of ECL signal amplifier for target molecule detection, which exhibit improved catalytic activity and enhanced ECL signal intensity [39,40]. Characterized by a large active surface area, superior electrocatalytic property, and excellent adsorption, triangular silver nanosheets (Tri-SNSs) can efficiently provide many active sites that exhibit a desirable catalytic performance for the ECL signal amplification of $Ru(bpy)_3^{2+}$/TPA [41].

In the present study, the sensing platform is first developed by assembling CS to the electrode, which is functionalized with 3D-ERGO via the amperometric I–T curve method. Subsequently, a signal-amplifier, Tri-SNSs, are employed to fix on the surface of 3D-ERGO. In addition, the ECL of the electrode during modification is investigated using the comparative experiment, which reveals that Tri-SNSs effectively enhance the ECL signal. Moreover, self-designed dual-$Ru(bpy)_3^{2+}$ scDNA (Ru_2-DNA) as probe for DNA hybridization is subsequently introduced on the electrode to release a strong ECL in the system. By the hybridization of Ru_2-DNA and t-DNA, force is markedly reduced, thereby inhibiting the ECL, leading to an ECL strategy for t-DNA detection. The diagram for the ultrasensitive detection of t-DNA is illustrated in Scheme 1.

2. Experimental section

2.1. Apparatus

The ECL emission detection was carried out with a computerized MPI-B type ultra-weak luminescence analyzer (Xi' An Remax Electronic Science Tech. Co. Ltd. Xi' An, China) equipped with a photomultiplier. The voltage of the photomultiplier tube (PMT) was set at -800 V. A conventional three-electrode system with a modified

GCE (3 mm in diameter) as the working electrode, a platinum wire as auxiliary electrode and Ag/AgCl electrode as reference electrode was used. Cyclic voltammetry (CV) experiments and electrochemical impedance spectroscopy (EIS) were measured with an IM6ex electrochemical workstation (Zahner IM6ex, Germany). All the measurements were carried out at room temperature. EIS was performed under an oscillation potential of 0.214 V over the frequency range of 1 Hz to 1 MHz. The amplitude of the alternate voltage was 5 mV. The electrochemical measurements (CV, EIS) were performed in the solution of 5 mM $[Fe(CN)_6]^{3-/4-}$ containing 0.1 M KCl solution. Ultraviolet-visible (UV-vis) absorption spectra were recorded on a Lambda 950 spectrophotometer (Perkin Elmer, U.S.A). Infrared spectra were collected with a Fourier transform infrared spectrophotometer (FT-IR, Nicolet iS50, USA). Atomic force microscopy (AFM) image was obtained by tapping-mode on a Nanoscope IIIa Digital Instruments with NSC15 tips (Veeco, CA, U.S.A). The morphologies of different nanomaterials were characterized by using a transmission electron microscope (TEM, JEM-1400, JEOL, Japan) and a scanning electron microscope (SEM, JSM-6360LA, JEOL, Japan). Raman spectra were recorded on a Jobin Yvon LABRAM-HR confocal laser micro-Raman spectrometer (Jobin Yvon, France) at room temperature and an excitation wavelength of 532 nm. X-ray diffraction (XRD) patterns was performed with a D8-Advance X-ray diffractometer (Bruker, Germany) operation using Cu Kα radiation.

2.2. Preparation of ECL probe and materials

Ru_2-DNA was synthesized by $Ru(bpy)_2(dcbpy)NHS$ and N_2-DNA in accordance with a previous study [42,43]. $Ru(bpy)_2(dcbpy)NHS$ was synthesized with some modification according to our previous work [44] and directly used to mark the $(NH_2)_2$-DNA (abbreviated as N_2-DNA) to obtain the double Beacon ECL probe (double $Ru(bpy)_2(dcbpy)NHS$ labeled N_2-DNA, abbreviated as Ru_2-DNA). Details on the synthesis steps and characterization results of Ru_2-DNA are provided in Supplementary Information.

The DNA oligonucleotide sequences for DNA probes and their targets as

presented as follows:

N_2-DNA: 5′ -NH_2-$(CH_2)_6$- GTGTGTGTGTGGTGTGG -$(CH_2)_6$-NH_2-3′

t-DNA: 5′-CCACACCACACACACAC -3′

M1-DNA: 5′-CAACACCACACACAC**T**C-3′

M2-DNA: 5′-CAACACCACACAC**T**C**T**C-3′

M4-DNA: 5′-CCACACCAC**T**C**T**C**T**C**T**C-3′

M6-DNA: 5′-CCACA**G**C**T**C**T**C**T**C**T**C-3′

M-DNA: 5′-**GGTGTGGTGTGTGTGTG**-3′

All aforementioned DNA oligonucleotides were purchased from Shanghai Sangon Biotechnology Co., Ltd. (Shanghai, China). Oligonucleotide probe was functionalized at both 5′ and 3′ end with an amino group, represented as N_2-DNA, The underlining section of t-DNA is complementary to N_2-DNA. The single-base mismatched (M1), two-base mismatched (M2), four-base mismatched (M4), six-base mismatched (M6), and all-base mismatched (M) DNA sequences of N_2-DNA correspond to t-DNA of different sequences. The mismatched bases are set in bold.

Graphene oxide (GO) was prepared by chemical exfoliation of natural flake graphite by using a modified Hummer's method [45] (see Supplementary Information for more details) and was dispersed in 0.1 M phosphate buffer solution (PBS) solution containing 0.1 M $LiClO_4$. The mass concentration of the obtained aqueous GO dispersion was estimated to be 2 mg/mL.

Tri-SNSs were typically prepared by reducing the $AgNO_3$ with $NaBH_4$ as a reductant in the presence of sodium citrate, polyvinylpyrrolidone (PVP), and H_2O_2 [46]. Tri-SNSs were presented as follows: 100 μL of 50 mM $AgNO_3$, 1.0 mL of 75 mM sodium citrate, 500 μL of 17.5 mM PVP, and 120 μL of 30% H_2O_2 were added to a 50 mL beaker with 38 mL distilled water in that sequence and then blended well under magnetic stirring. Subsequently, 400 μL of 100 mM $NaBH_4$ (ice water) was quickly added. It took almost 25 min for the entire transition from spherical nanoparticles to nanosheets. Tri-SNSs in a blue mother solution were subsequently characterized by TEM.

2.3. Construction of modified electrodes

Prior to modification, a glassy carbon electrode (GCE) with a diameter of 3 mm, which was used in the experiment, was first polished using α-Al_2O_3 powder, followed by sonication in deionized water, absolute ethyl alcohol, and deionized water. The GCE was then transferred to a 0.5 M H_2SO_4 solution and a 5 mM $[Fe(CN)_6]^{3-/4-}$ probe for further activation and characterization. 3D-ERGO was formed on the surface of the GCE by adopting the amperometric I–T curve method for 600 s. Approximately 4 uL of CS solution (0.001%) was dropped on the surface of 3D-ERGO/GCE to reinforce the 3D framework and the stability between 3D-ERGO and the GCE. The 3D-ERGO/GCE was then dried in N_2 flow. Subsequently, 3 μL Tri-SNSs blue solution was covered on the surface and dried in N_2 in a dry room. The CS/3D-ERGO/GCE was then immersed into 1 mM 2-mercaptobenzothiazole for 5 min to accelerate the formation of Ag–S bonds. Finally, Ru_2-DNA as an ECL probe was self-assembled on the surface of the Tri-SNSs/CS/3D-ERGO/GCE by non -covalent attraction, which was regarded as Ru_2-DNA/Tri-SNSs/CS/3D-ERGO/GCE.

2.4. ECL experiment of biosensor

The as-prepared Ru_2-DNA/Tri-SNSs/CS/3D-ERGO/GCE was added into 200 μL 0.1 M PBS solution containing varying concentrations of t-DNA and then incubated at room temperature, followed by thorough washing in 0.1 M PBS to remove formative dcDNA, which consists of Ru_2-DNA and t-DNA by complementary base pairing. Determination of ECL was conducted at room temperature in a 0.1 M PBS solution containing 0.1 M TPA. CV mode was adopted with continuous potential scanning from 0.2 V to 1.25 V at a scanning rate of 100 $mV \cdot s^{-1}$ with a photomultiplier tube voltage of 800 V. The content of the target was determined in accordance with the variation in ECL peak intensity from ECL peak intensity with no target. ΔI_{ECL} ($\Delta I=(I_0-I)/I_0$), where I_0 and I denote the average ECL intensity of these blank tests and the ECL intensity of detection limit, respectively.

3. Results and discussion

3.1. Characterization of GO

GO was synthesized from graphite by adopting Hummers' method, which was confirmed by XRD, SEM, TEM, U-vis, and AFM. Compared with that of graphite, the peak of GO appears at 10.0° (Fig. S2A) because the armchair-type stacking order was still observed in GO with a carbon interlayer spacing of 0.883 nm [47]. This value is larger than that of G, which was 0.336 nm (2 theta. 26.5°). The difference was attributed to the unfolding of the interlayer [48]. SEM and TEM (Fig. S2B, C) could be used to verify the effect of the method of preparing GO. The as-prepared GO appeared wrinkled, which is consistent with the finding in the literature [49]. Meanwhile, UV-vis showed 2 main features (Fig. S2D): a peak at 230 nm and a shoulder at 300 nm. The former corresponds to the π–π* transition of aromatic C-C bonds, whereas the latter was attributed to the π–π* transition of the C=O bonds. AFM (Fig. S2E) showed that the monodisperse thickness of GO was about 0.95 nm. The edge showed the marked shapes, and the roughness further proved this result. All characterization techniques indicated that a considerably thin single-layer GO was obtained.

3.2. Characterization of Tri-SNSs

TEM was conducted for the intuitive characterization of Tri-SNSs. Most nanosheets exhibited a clean-cut triangular structure, with an average edge length of about 25 nm (Fig. 1A). In addition, several nanosheets in the insert tend to appear stacked face-to-face and stand perpendicularly on their edges. This appearance facilitates the calculation of their thickness and reveals the uniform thickness of 4 nm for Tri-SNSs. The distribution of particles is presented in Fig. S3. In Fig. 1B, the lattice patterns of Tri-SNSs clearly showed a lattice spacing of 0.21 nm. Comparative diagrams of TEM for Tri-SNSs with or without PVP were also recorded (Fig. 1C, 1D). However, the product without PVP only contained spherical and plate-like nanoparticles, as well as morphological nanoparticles. This occurrence

confirmed the stabilizing effect of PVP and clearly demonstrated that PVP could protect the anisotropic structures of Tri-SNSs from excessive corrosion of H_2O_2.

3.3. Characterization of composite electrode assembly

The chemical characteristics and material texture of interfacial modification was examined by FT–IR, raman spectroscopy, and SEM. In Fig. S5A, The characteristic peak of the O-H (3415.79 cm^{-1}), C=C (1624.67 cm^{-1}), C=O (1735.35 cm^{-1}), and C-O-C (1077.88 cm^{-1}) groups in GO are clearly marked. Compared with GO/GCE, all peaks of the oxidizing group on 3D-ERGO/GCE were significantly decreased, followed by a reduction in electrodeposition, which indicated that oxygenous groups on GO were removed to a large extent. As shown in Fig. S5B, the Raman spectra were also studied to discuss modified electrodes. The band around 1350 cm^{-1} was the D-band of carbon authenticated as the structural deficiency or partially disordered graphite domains. The band near 1600 cm^{-1} is the G-band of carbon representing the graphite domains [50]. The rate of intensity between D-bands and G-bands (I_D/I_G) can be used to calculate the average dimension of crystalline sp^2 domains and further analyze the degree of oxidation of carbon materials. Compared with GO (b), the G band of 3D-ERGO was markedly higher than the D band (c), which indicated that GO was reduced to RGO to a large extent. The Raman intensity of CS/3D-ERGO/GCE (d) was greater than that of 3D-ERGO/GCE (c), which was attributed to the blocking effect of CS on the Raman response of the materials. The intensity of the D-band and G-band Tri-SNSs/CS/3D-ERGO/GCE (e) was markedly enhanced, which could be attributed to the charge transfer from the Tri-SNSs to the graphene in accordance with previous reports [51, 52].

The morphologies of the as-prepared 3D-ERGO/GCE and Tri-SNSs/CS/3D-ERGO/GCE were examined by SEM (Fig. 2). In Fig. 2A, owing to the drive of the electric field and hydrophobic interactions, a large amount of 3D-ERGO appeared crowded on the surface of the electrodes and exhibited an interconnected 3D network structure via self-assembly, clearly revealing the high specific surface area of 3D-ERGO. This approach effectively formed 3D graphene

structures on the GCE by using 2 mg/mL of GO dispersion liquid as the electrodeposition system and the amperometric I–T curve method as the deposition technique. Meanwhile, the effect of the variation in deposition times was evaluated (Fig. S6). The details are provided in Supplementary Information. Owing to the electronic insulation properties of CS, the SEM image of Tri-SNSs/CS/3D-ERGO/GCE (Fig. 2B) presented a fuzzy vision. Tri-SNSs were also evenly distributed on the surface of the modified electrodes.

Energy dispersive spectrometer (EDS) of Tri-SNSs/CS/3D-ERGO/GCE was subsequently recorded (Fig. S7). Elemental analysis indicated the following: C atom, 79.58%; O atom, 9.90%; and Ag atom, 10.52%.

3.4. Electrochemical measurement of modified electrodes

CV and EIS were employed to confirm the process of electrode modification (Fig. S8). CV of the bare GCE showed one current at 0.93×10^{-4} A (curve a), and reached 1.77×10^{-4} A (curve b) after the electrodeposition of 3D-ERGO. Immediately after subsequent modification, the current decreased (curves c–e). However, the current of the electrode suddenly rose to 1.23×10^{-4} A (curve f) when the modified electrode was taken to incubate with a specific concentration of the t-DNA solution (Fig. S8A). The semicircle diameters at the high-frequency region reflect the electron transfer resistance (Ret), which is associated with the electron transfer kinetics of the redox probe at the electrode interface, whereas the linear part at lower frequencies corresponds to the diffusion resistance (Fig. S8B) [7]. The Nyquist plot (curve a) of the bare GCE showed an extremely small semi-circle . Following the introduction of 3D-ERGO on the surface, the semi-circle became smaller and less than 100 Ω because of the electrical conduction enhancement. When CS, Tri-SNSs, and Ru_2-DNA were sequentially modified on the GCE surface (curves c–e), the Ret value was markedly decreased. This reduction could be attributed to the negatively charged and electrical insulating properties of subsequent substances, which repelled $[Fe(CN)6]^{3-/4-}$ and inhibited the electron transfer. Thus, the semi-circle considerably decreased after the incubation of t-DNA (f) [31].

3.5. ECL measurement and reaction mechanism of modified electrodes

ECL testing was used to distinguish the assembly effect of different composite electrodes by comparing the ECL peak of scanning curves. As is shown in Fig. 3, almost no ECL signal was generated on Tri-SNSs/CS/3D-ERGO/GCE in the absence of $Ru(bpy)_3^{2+}$. However, both 3D-ERGO and Tri-SNSs exhibited excellent ECL amplification in the $Ru(bpy)_3^{2+}$/TPA system. Therefore, Tri-SNSs/CS/3D-ERGO/GCE can effectively promote the $Ru(bpy)_3^{2+}$/TPA system to release the ECL signal. Such a modified electrode was suitable for the ultrasensitive determination of t-DNA concentration.

Moreover, the possible reaction mechanisms is shown below:

$H_2O\text{-}e \rightarrow H^+ + OH\cdot$ (1)

$Tri\text{-}SNSs + TPA \rightarrow Tri\text{-}SNSs(TPA)$ (2)

$Tri\text{-}SNSs(TPA) + OH\cdot \rightarrow Tri\text{-}SNSs(TPA\cdot) + OH^-$ (3)

$Ru(bpy)_3^{2+}\text{-}e\text{-} \rightarrow Ru(bpy)_3^{3+}$ (4)

$Ru(bpy)_3^{3+} + Tri\text{-}SNSs(TPA\cdot) \rightarrow [Ru(bpy)_3^{2+}]^* + Tri\text{-}SNSs + Product$ (5)

$[Ru(bpy)_3^{2+}]^* \rightarrow Ru(bpy)_3^{2+} + h\nu$ (orange-red glow) (6)

H_2O may be oxidized to OH· (Eq. (1)) when the applied positive potential scan (PPS) is larger than the valance band of H_2O. TPA is easily absorbed on the surface of Tri-SNSs to form Tri-SNSs (TPA) by the interface energy of the nanomaterial (Eq. (2)). Under oxidation potential, the surface of Tri-SNSs became a active sites for TPA absorption; OH· is then intended to generate a mass of TPA· upon Tri-SNSs (TPA) (Eq. (3)). TPA in the solution can also be translated into TPA·, which fuels $[Ru(bpy)_3^{2+}]^*$ and generates (Eq. (5)). The entire process relies on ECL resonance energy transfer and the redox reaction among $Ru(bpy)_3^{2+}$, TPA, and composite electrodes.

3.6. Analytical property of ECL biosensor for t-DNA detection

The potential quantitative application and the sensitivity of the as-prepared ECL biosensors with varying concentrations of t-DNA was investigated. In Fig. 4A, ECL intensity weakened with increasing concentration of t-DNA, which was measured in

0.1 M PBS containing 0.1 M TPA at 100 $mV \cdot s^{-1}$. ΔI_{ECL} was found to be logarithmically related to the concentration of t-DNA in the 100 aM to 100 pM range (Fig. 4B). The regression equation is expressed as $\Delta I_{ECL} = \Delta I/I_0 = 0.13231 \lg c_{(t\text{-}DNA)} + 0.7048$ ($\Delta I/I_0$, ($\Delta I = I_0 - I$)) with a regression coefficient of 0.9959 and a limit of detection (LOD) of 16.2 aM, which is estimated from the derived calibration curve (>3 standard deviations (SD)). This result indicated that the use of the ECL biosensor is a suitable and potential method for t-DNA detection.

Comparison of the analytical performance of the proposed method with that of other reported methods in DNA detection is presented in Table S1. Healthy human serum samples with varying amounts of t-DNA were prepared and measured. The results in Table S2 show satisfactory quantitative recovery, which revealed that the ECL DNA biosensor could perform efficiently and was certainly a satisfactory method for DNA detection in real biological samples.

3.7. ECL stability, reproducibility, and specificity of the proposed biosensor

The ECL signal–time curve under continuous potential scanning for a long period is presented in Fig. 5A. The result indicates that the ECL intensity was stable, suggesting that the proposed biosensor exhibited a considerably satisfactory ECL response to DNA detection. Meanwhile, the percentage of ECL intensity gradually decreased to about 91.0% of its initial value after being stored in darkness at 4 °C for 30 days. The stability of the proposed biosensor at different concentrations of t-DNA was evaluated. The ECL signal intensity decreased with increasing concentration of t-DNA (Fig. 5B). In addition, these results verify that this sensing strategy was satisfactory and feasible.

Moreover, 100 pM of t-DNA, M1-DNA, M2-DNA, M4-DNA, M6-DNA, and M-DNA were detected in the ECL testing system to investigate the specification of the proposed biosensor, which is presented in Fig. 5C. The highest increase in ECL occurred after hybridization with M6-DNA and M-DNA. Nevertheless, compared with the blank sample, a slight reduction in ECL attenuation was observed when

hybridization with M2-DNA and M4-DNA occurred. Notably, M1-DNA in ECL testing led to an apparent reduction although the decrease is much higher than that of t-DNA. In addition, M1-DNA could be easier to distinguish t-DNA from M2-DNA, indicating that our method provides high specificity and could be clearly applied to DNA testing.

These results suggest that the proposed biosensor electrode have a good ECL stability, reproducibility, and specificity.

Within-run precision and between-run precision were investigated to verify the reproducibility of the biosensor for t-DNA detection. The proposed electrode was evaluated by measuring one t-DNA level for five repetitive trials, and with five DNA biosensors produced on the same electrode. The relative standard deviations (RSD) of within-run precision and between-run precision obtained from 1 fM t-DNA were 5.2% and 6.0%, respectively, which indicated satisfactory precision and reproducibility of fabrication.

3.8. Optimization of the proposed biosensor

To obtain desirable ECL quenching, the influences of pH, incubation time of Ru_2-DNA, and incubation time of t-DNA on the performance of the biosensor were investigated individually. In Fig. S9A, ECL intensity increases with increasing pH, obtaining the maximum at pH of 7.4. This occurrence could be attributed to the stability of the reaction of the whole system at pH 7.4, which contributed to the amplification of ECL emission. The influence of the incubation time of Ru_2-DNA is given in Fig. S9B. Therefore, a certain period of Ru_2-DNA incubation contributed to the amplification of ECL emission and reached the plateau at 180 min. ECL quenching was controlled by the loss of t-DNA to Ru_2-DNA from the electrode surface. ECL intensity markedly decreased with increasing t-DNA introduced and became nearly saturated at 4.0 h. Thus, 4.0 h could be chosen as the satisfactory incubation period (Fig. S9C). All ECL curves were measured in 0.1 M PBS containing 0.1 M TPA at 100 mV s^{-1}.

In order to verify that Ru_2-DNA has better ECL performance than Ru-DNA, ECL intensity of the proposed biosensor after modified Ru_2-DNA (a) and Ru-DNA (b) with 1 pM t-DNA (Fig. S10). The ECL curves were measured in 0.1 M PBS containing 0.1 M TPA at 100 mV s^{-1}. As we can see, the ECL of double sided $Ru(bpy)_3^{2+}$ modification is more beneficial than that of single sided modification (1: 0.63). Thus, double sided $Ru(bpy)_3^{2+}$ modification can effectively enhance the ECL signal in the application of biochemical analysis.

4. Conclusions

We report here a Tri-SNSs-layered, CS-supported three-dimensional of reduced graphene oxide ECL biosensing platform using Ru_2-DNA as capture probe for ECL biosensing of single-chain DNA (scDNA). By using such a ECL biosensing platform, the performance of electrochemistry and ECL for the detection of DNA were investigated by several technique, and showed that the proposed platform have not only exhibited favourable conductivity and ECL intensity than that of GCE due to 3D graphene framework and Tri-SNSs amplifier, but also provided a high sensing performances in DNA detection due to ECL strategy. Under optimal conditions, the ECL biosensor presents favorable sensitivity with high recovery and extremely low limit of LOD. Finally, stability, sensitivity, and specificity were also investigated to confirm the practicability of biosensors, which proves that a novel biosensor may provide a new application in ultrasensitive bioanalysis of DNA sequencing, diagnostic analysis, and disease control.

Acknowledgements

We are grateful for the financial support from the Natural Science Foundation of Guangdong Province (No. 2014A030313480), the Science & Technology Project of Guangdong Province (No. 2013B030600001 & No. 2016A020223014), and the National Natural Science Foundation of China (No. 51272152/E0208).

References

[1] J. P. Jia, S. S. Shi, R. N. Ma, W. L. Jia, H. S. Wang, Highly sensitive electrochemical biosensor based on nonlinear hybridization chain reaction for DNA detection, Biosens. Bioelectron. 80 (2016) 392–397.

[2] J. Zhang, H. L. Qi, Y. Li, J. Yang, Q. Gao, C. X. Zhang, Electrogenerated chemiluminescence DNA biosensor based on hairpin DNA probe labeled with ruthenium complex, Anal. Chem. 80 (2008) 2888–2894.

[3] X. Z. Wang, L. Ge, Y. F. Yu, S. S. Dong, F. Li, Highly sensitive electrogenerated chemiluminescence biosensor based on hybridization chain reaction and amplification of gold nanoparticles for DNA detection, Sens. Actuators. B. 220 (2015) 942–948.

[4] F. Lucarelli, A. Kicela, I. Palchetti, G. Marrazza, M. Mascini, Electrochemical DNA biosensor for analysis of wastewater samples, Bioelectrochem. 58 (2002) 113–118.

[5] X. L. Zuo, F. Xia, Y. Xiao, K. W. Plaxco, Sensitive and selective amplified fluorescence DNA detection based on exonuclease III-aided target recycling, J. Am. Chem. Soc. 132 (2010) 1816–1818.

[6] J. Xu, Z. S.Wu, W. Shen, H. Xu, H. Li, L. Jia, Cascade DNA nanomachine and exponential amplification biosensing, Biosens. Bioelectron. 73 (2015) 19−25.

[7] Z. Zhu, J. P. Lei, L. Liu, H. X. Ju, Label-free electrochemical DNA sensing with a one-target-multitriggered hybridization chain reaction strategy, Analyst. 138 (2013) 5995–6000.

[8] L.Yuan, W. W.Tu, J. C. Bao, Z. H. Dai, Versatile Biosensing Platform for DNA Detection Based on a DNAzyme and Restriction-Endonuclease-Assisted Recycling, Anal. Chem. 87 (2015) 686−692.

[9] J. Chen, H. Qiu, M. Zhang, T. Gu, S. Shao, Y. Huang, S. Zhao, Hairpin assembly-triggered cyclic activation of a DNA machine for label-free and ultrasensitive chemiluminescence detection of DNA, Biosens. Bioelectron. 68 (2015) 550−555.

[10] F. Zhang, H. Chen, P. G. He, Y. Z. Fang, Research on DNA electrochemiluminescence biosensing, J. Anal. Chem. 41 (2013) 1–9.

[11] G. F. Jie, Y. Q. Qin, Q. M. Meng, J. L. Wang, Autocatalytic amplified detection of DNA based on a CdSe quantum dot/folic acid electrochemiluminescence energy transfer system, Analyst.140 (2015) 79–82.

[12] D. Wang, G. Chen, H. Wang, W. Tang, W. Pan, N. Li, F. Liu, A reusable quartz crystal microbalance biosensor for highly specific detection of single-base DNA mutation, Biosens. Bioelectron. 48 (2013) 276–280.

[13] J. B. Wood, M. W. Szyndler, A. R. Halpern, K. Cho, R. M. Corn, Fabrication of DNA microarrays on polydopamine-modified gold thin films for SPR imaging measurements, Langmuir. 29 (2013) 10868–10873.

[14] F. Gao, J. Lei, H. Ju, Label-free surface-enhanced raman spectroscopy for sensitive DNA detection by DNA-mediated silver nanoparticle growth, Anal. Chem. 85 (2013) 11788–11793.

[15] A. C. Lee, J. S. Ye, S. N. Tan, D. P. Poenar, F. S. Sheu, C. K. Heng, T. M. Lim, Carbon nanotube-based labels for highly sensitive colorimetric and aggregation-based visual detection of nucleic acids, Nanotechnology. 18 (2007) 455102.

[16] D. M. Hereules, F. E. Lytle, Chemiluminescence from reduction reactions, J. Am. Chem. Soc. 88 (1966) 4745-4746.

[17] X. Li, S. Yu, T. Yan, Y. Zhang, B. Du, D. Wu, Q. Wei, A Sensitive Electrochemiluminescence Immunosensor Based on $Ru(bpy)_{32+}$ in 3D CuNi Oxalate as Luminophores and Graphene Oxide-Polyethylenimine as Released $Ru(bpy)_{32+}$ Initiator, Biosens. Bioelectron. 89 (2017) 1020–1025.

[18] S. Tsuneyasu, R. Takahashi, H. Minami, K. Nakamura, N. Kobayashi, Ultrafast Response in AC-Driven Electrochemiluminescent Cell Using Electrochemically Active DNA/$Ru(bpy)_3^{2+}$ Hybrid Film with Mesoscopic Structures, Sci. Rep. 7 (2017) 8525.

[19] L. J. Liang, W. Hu, Z. Y. Xue, J. W. Shen, Theoretical study on the interaction of nucleotides on two-dimensional atomically thin graphene and molybdenum disulfide, Flat. Chem. 2 (2017) 8–14.

[20] Y. Wang, Y. Li, L. Tang, J. Lu, J. Li, Application of graphene-modified electrode for selective detection of dopamine, Electrochem. Comm. 11 (2009) 889–892.

[21] C. Bosch-Navarro, Z. P. L. Laker, A. J. Marsden, N. R. Wilson, J. P. Rourke, Flat. Chem. 1 (2016) 52–56.

[22] M. D. Stoller, S. Park, Y. Zhu, J. An,R. S. Ruoff, Graphene-based ultracapacitors, Nano. Lett. 8 (2008) 3498–3502.

[23] Y. X. Xu, G. Q. Shi, Assembly of chemically modified graphene: methods and applications, J. Mater. Chem. 21 (2011) 3311–3323.

[24] C. Mattevi, H. Kim, M. Chhowalla, A review of chemical vapour deposition of graphene on copper, J. Mater. Chem. 21 (2011) 3324–3334.

[25] K. S. Novoselov, A. K. Geim, S. V. Morozov, D. Jiang, Y. Zhang, S. V. Dubonos, I. V. Grigorieva, A. A. Firsov, Sci. 306 (2004), 666–669.

[26] C. Lee, X. Wei, J. W. Kysar, J. Hone, Measurement of the elastic properties and intrinsic strength of monolayer graphene, Science. 321 (2008) 385–388.

[27] S. J. He, B. Song, D. Li, C. F. Zhu, W. P. Qi, Y. Q. Wen, L. H. Wang, S. P. Song, H. P. Fang, C. H. Fan, A graphene nanoprobe for rapid, sensitive, and multicolor fluorescent DNA analysis, Adv. Funct. Mater.20 (2010) 453–459.

[28] B. Partoens, F. M. Peeters, From graphene to graphite: Electronic structure around the K point, Phys. Rev. B.74 (2006) 075404.

[29] S. Nardecchia, D. Carriazo, M. L. Ferrer, Three dimensional macroporous architectures and aerogels built of carbon nanotubes and/or graphene: synthesis and applications, Chem. Soc. Rev. 42 (2013) 794–830.

[30] L. Jiang, Z. Fan, Design of advanced porous graphene materials: from graphene nanomesh to 3D architectures, Nanoscale. 6 (2014) 1922–1945.

[31] j. Zhang,Y. Sun, H. Zhang, B. Xu, H. Zhang, D. Song, Preparation and application of triangular silver nanoplates/chitosan composite in surface plasmon resonance biosensing, Anal. Chem. Acta. 769 (2013) 114–120.

[32] M. Chen, C. Zhang, X. Li, L. Zhang, Y. Ma, L. Zhang, X. Xu, F. Xia, W. Wang, J. Gao, A one-step method for reduction and self-assembling of graphene oxide into reduced graphene oxide aerogels, J. Mater. Chem. A. 1 (2013) 2869–2877.

[33] Z. Han, Z.Tang, P, Li, G. Yang, Q. Zheng, J. Yang, Ammonia solution strengthened three-dimensional macro-porous graphene aerogel, Nanoscale. 5 (2013)

5462–5467.

[34] Z. Chen, W. Ren, L, Gao, B. Liu, S. Pei, H. M. Cheng, Three-dimensional flexible and conductive interconnected graphene networks grown by chemical vapour deposition, Nat. mater. 10 (2011) 424–428.

[35] J. Wang, Electrochemical nucleic acid biosensors, Anal. Chim. Acta. 469 (2002) 63–71.

[36] S. Takenaka, K. Yakenaka, M. Takagi, Y. Uto, H. Kondo, DNA sensing on a DNA probe-modified electrode using ferrocenylnaphthalene diimide as the electrochemically active ligand, Anal. Chem. 72 (2000) 1334–1341.

[37] J. Olejnik, E. Krzymanska-Olejnik, K. J. Rothschild, Photocleavable aminotag phosphoramidites for 5′-termini DNA/RNA labeling, Nucleic Acids Res. 26 (1998) 3572–3576.

[38] H. Hayatsu, Y. Tanaka, K. Negishi, Preparation of DNA-chitosan columns and their applications: binding of carcinogens to the column, Nucleic Acids Symp. Ser. 37 (1997) 139–140.

[39] X. Du, D. Jiang, Q. Liu, J. Qian, H. Mao, K. Wang, Enhanced electrochemiluminescence sensing platform using nitrogen-doped graphene as a novel two-dimensional mat of silver nanoparticles, Talanta. 132 (2015) 146–149.

[40] H. T. Chou, C. U. Fu, C. Y. Lee, N. H. Tai, H. Y. Chang, An ultrasensitive sandwich type electrochemiluminescence immunosensor for triiodothyronine detection using silver nanoparticle-decorated graphene oxide as a nanocarrier, Biosens. Bioelectron. 71 (2015) 476–482.

[41] L. Mulfinger, S. D. Solomon, M. Bahadory, A. V. Jeyarajasingam, S. A. Rutkowsky, C. Boritz, Synthesis and study of silver nanoparticles, J. Chem. Educ. 84 (2007) 322.

[42] G. Sprintschnik, H. W. Sprintschnik, P. P. Kirsch, D. G. Whitten, Photochemical reactions in organized monolayer assemblies. 6. Preparation and photochemical reactivity of surfactant ruthenium (II) complexes in monolayer assemblies and at water-solid interfaces, J. Am. Chem. Soc. 99 (1977) 4947–4954.

[43] E. Terpetsching, H. Szmacinski, H. Malak, J. R. Lakowicz, Metal-ligand

complexes as a new class of long-lived fluorophores for protein hydrodynamics, Biophysical. Journal. 68 (1995) 342–350.

[44] W. H. Gao, A. Zhang, Y. S. Chen, Y. W. Chen, F. S. Lu, G. Z. Chen, Biosens. Bioelectron. 49 (2013) 139-145.

[45] N. I. Kovtyukhova, P. J. Ollivier, B. R. Martin, T. E. Mallouk, S. A. Chizhik, E. V. Buzaneva, A. D. Gorchinskiy, Layer-by-layer assembly of ultrathin composite films from micron-sized graphite oxide sheets and polycations, Chem. Mater. 11 (1999) 771–778.

[46] J. Zhang, F. Zhao, Z. Zhang, Dimension-tailored functional graphene structures for energy conversion and storage, Nanoscale. 5 (2013) 3112–3126.

[47] Y. X. Xu, H. H. G. W Lu, C. Li, G. Q. Shi, Flexible graphene films via the filtration of water-soluble noncovalent functionalized graphene sheets, J. Am. Chem. Soc. 130 (2008) 5856–5857.

[48] D. C. Marcano, D. V. Kosynkin, J. M Berlin, A. Sinitskii, Z. Sun, A. Slesarey, L. B. Alemary, W. Lu, J. M. Tour, Improved synthesis of graphene oxide, ACS. Nano. 4 (2010) 4806–4814.

[49] Z. Luo, Y. Lu, L. A. Somers, A. C. Johnson, High yield preparation of macroscopic graphene oxide membranes, J. Am. Chem. Soc. 131 (2009) 898–899.

[50] K. B. Kudin, B. Ozbas, H. C. Schniepp, R. K. Prud'homme, I. A. Asksay, R. Car, Raman spectra of graphite oxide and functionalized graphene sheets, 8 (2008) 36–41.

[51] S. Lin, W. Zhu, Y. Jin, K. B. Crozier, Surface-enhanced Raman scattering with Ag nanoparticles optically trapped by a photonic crystal cavity, Nano. Letters. 13 (2013) 559–563.

[52] L. Gan, M. Yang, X. Ke, G. Cui, X. Chen, S. Gupta, G. Wu, Mesoporous Ag nanocubes synthesized via selectively oxidative etching at room temperature for surface-enhanced Raman spectroscopy, Nano. Res. 8 (2015) 2351–2362.

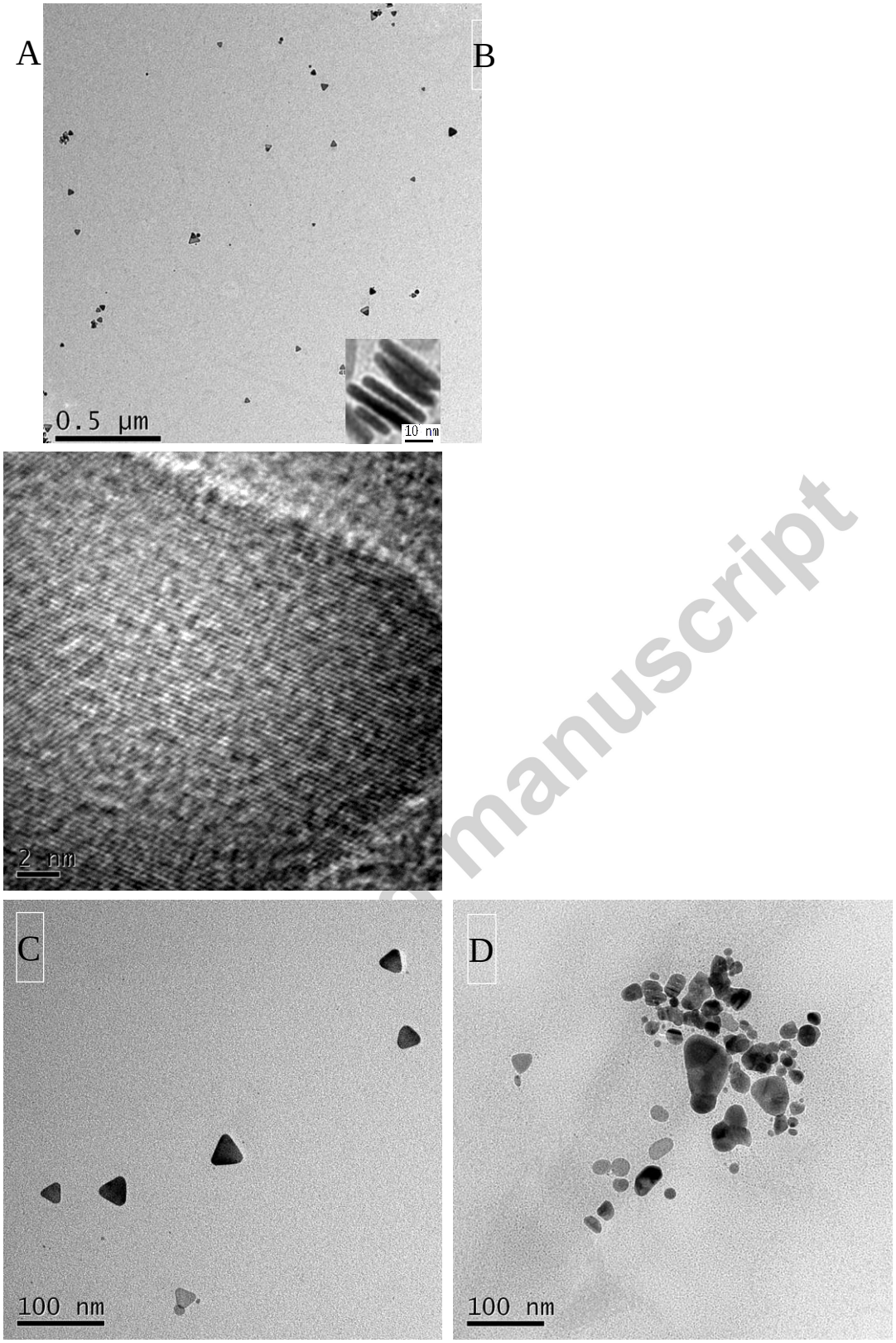

Fig. 1 TEM of Tri-SNSs prepared in the presence of PVP (Illustrations: the profile morphology of SNSs) (A), HRTEM image of Tri-SNSs (B), TEM of SNSs with PVP (C) without PVP(D).

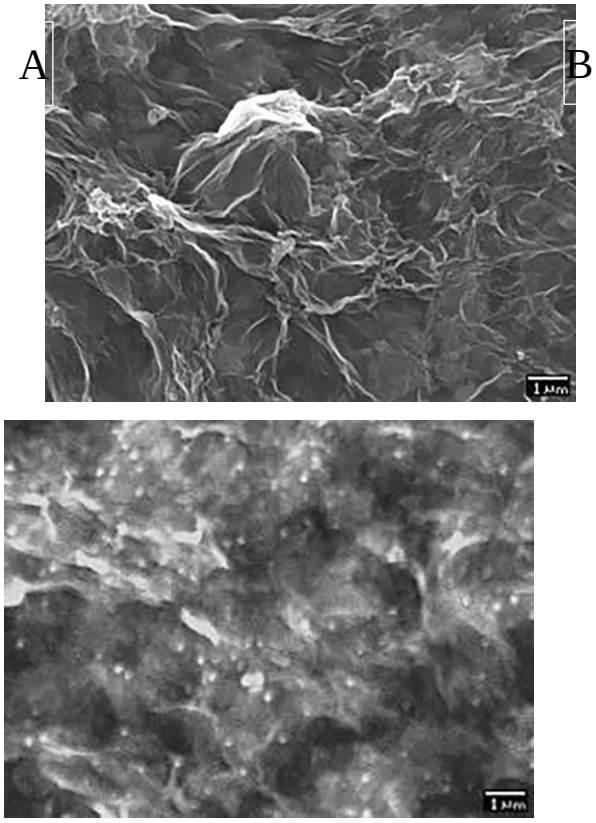

Fig. 2 SEM image of 3D-ERGO/GCE (A) and Tri-SNSs/CS/3D-ERGO/GCE (B)

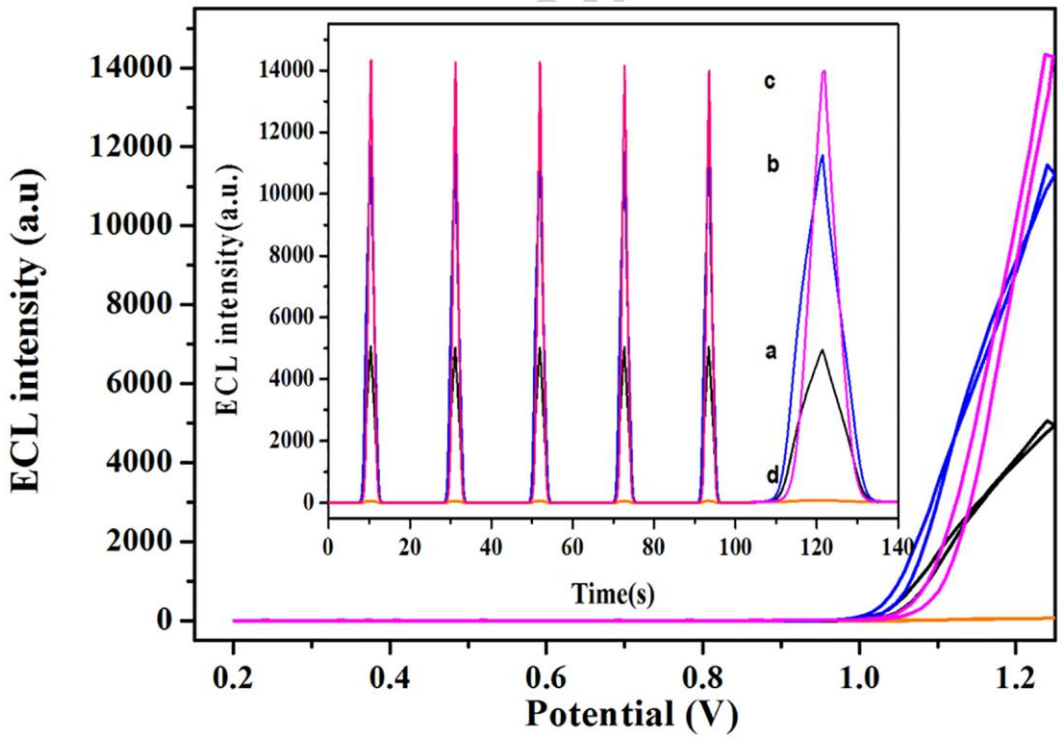

Fig. 3 ECL intensity vs. potential curve for GCE (a), 3D-ERGO/GCE (b), Tri-SNSs/CS/3D-ERGO/GCE (c), Tri-SNSs/CS3D-ERGO/GCE (d) was measured in the absence

of $Ru(bpy)_3^{2+}$. Inset: ECL intensity vs. time curves for continuous CV for 5 cycles ECL testing were measured in 0.1 M PBS (pH, 7.4) containing 1 μM $Ru(bpy)_3^{2+}$ and 0.1M TPA at 100 $mV \cdot s^{-1}$;

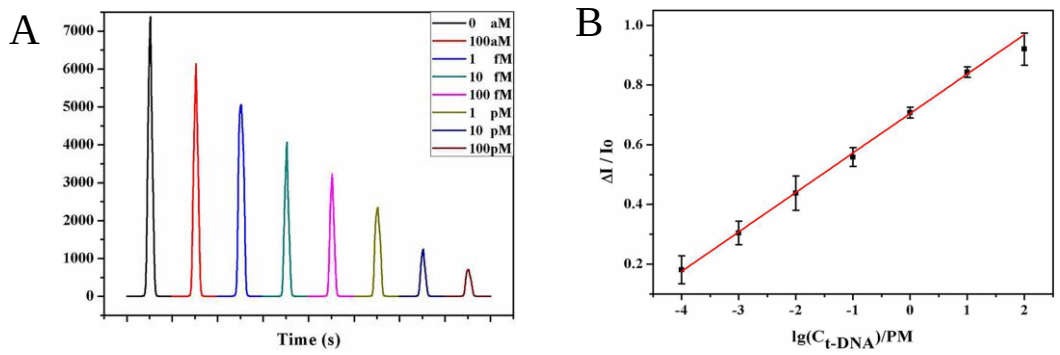

Fig. 4 (A) ECL signal intensity of the biosensor with different concentration of t-DNA, (B) Linear relationship between ECL intensity (ΔI_{ECL}) and log of the t-DNA concentrations.

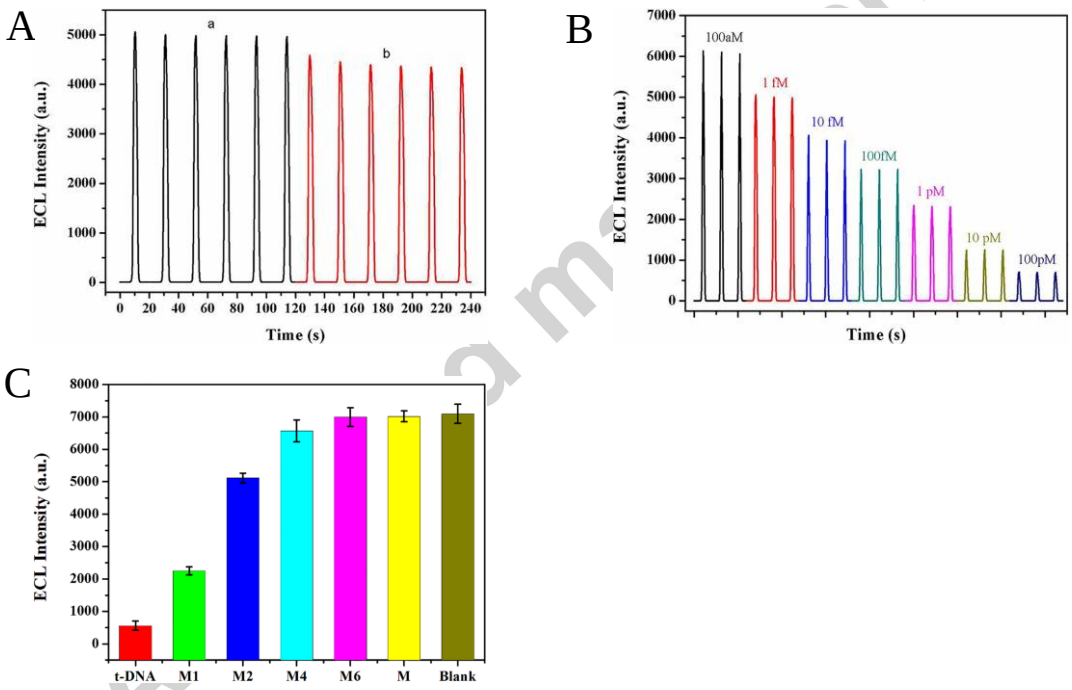

Fig. 5 (A) ECL intensity of the proposed biosensor after 30 days with 1 fM t-DNA; (B) Stability of the biosensor with different concentration of t-DNA in 0.1 M PBS containing 0.1 M TPA at 100 $mV \cdot s^{-1}$; (C) Specificity of the proposed biosensor: 100 pM t-DNA, M1-DNA, M2-DNA, M4-DNA, M6-DNA, M-DNA, 0 pM t-DNA. The error bars represent the standard deviation of three measurements and ECL were measured in 0.1 M PBS containing 0.1 M TPA at 100 $mV \cdot s^{-1}$.

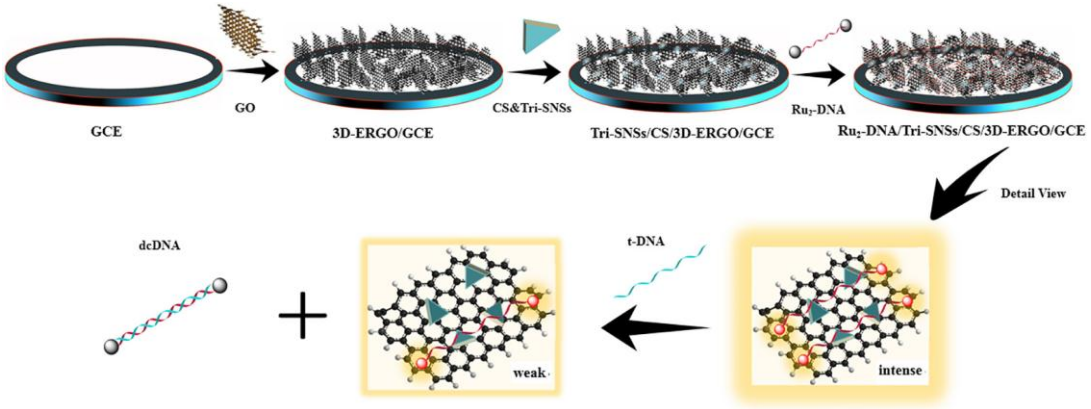

Scheme. 1 Schematic representation of the ECL biosensor preparation and response process

Highlights

- A wide and stable platform for Ru_2-DNA adsorption based on 3D electro-deposited reduced graphene oxide is designed.
- First to adopt triangle silver nano-sheets (Tri-SNSs) as ECL signal amplifier for DNA detection.
- Self-designed dual-$Ru(bpy)_3^{2+}$ scDNA is synthesized, thereby improving the number of luminous beacon on biosensing platform and increased the ECL signal.
- Provide an effective way to distinguish DNA sequence.
- This work suggests that the biosensor what we designed serves as a promising choice for the field of bioanalysis.

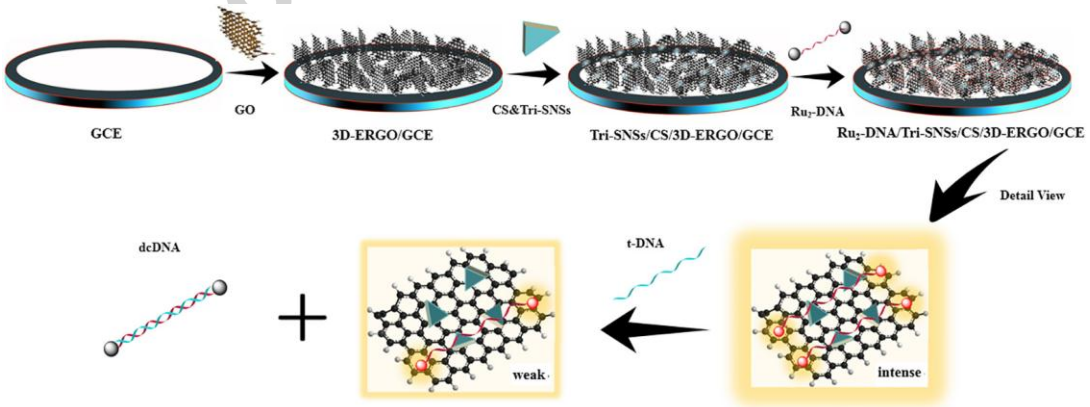

Graphical abstract